Inorganica Chimica Acta 561 (2024) 121844

Contents lists available at ScienceDirect

Inorganica Chimica Acta

journal homepage: www.elsevier.com/locate/ica

Geometric control of Cu, Ni and Pd complexes in the solid state via intramolecular H-bonding interactions

Ankita Puri [a], Allison McAninch [a], Sheng Shu [a], Khashayar Rajabimoghadam [b], Maxime A. Siegler [c], Marcel Swart [d,e,*], Isaac Garcia-Bosch [a,*]

[a] Department of Chemistry, Carnegie Mellon University, Pittsburgh, PA 15213, United States
[b] Department of Chemistry, Southern Methodist University, Dallas, TX 75275, United States
[c] Johns Hopkins University, Baltimore, MD 21218, United States
[d] University of Girona, Campus Montilivi (Ciències), IQCC, Girona, Spain
[e] ICREA, Pg. Lluís Companys 23, 08010 Barcelona, Spain

ARTICLE INFO

Keywords:
Coordination complexes
Intramolecular H-bonding interactions
Copper
Nickel
Palladium
Single crystal X-ray diffraction analysis

ABSTRACT

In this article, we describe the synthesis and characterization of a family of copper, nickel and palladium complexes bound by bidentate ligands derived from *ortho*-phenylenediamine that contain tunable H-bond donors. The crystal structures of the reduced dianionic metal complexes (formulated as $[M^{II}(L^{2-})_2]^{2-}$) depict intramolecular H-bonding interaction between the two ligand scaffolds. Variations on the primary (Cu, Ni, Pd), secondary (H-bonding donor) and tertiary coordination sphere (solvent of crystallization and countercation), led to the isolation of the metal complexes in square-planar (SP) and/or twisted pseudo-tetrahedral geometry (TW). A detailed structural analysis of the complexes in the solid state revealed that the intramolecular H-bonding interactions can be altered by disrupting the bonds between the countercation, solvent of crystallization and the ligand scaffold, which leads to changes in the geometry of the complexes (SP or TW). DFT calculations are in agreement with our experimental observations, in which the Cu complexes were found to favor twisted geometries while the Ni and Pd complexes favored square-planar geometries.

1. Introduction

The structure, spectroscopy and reactivity of metal complexes are usually tuned by varying the primary coordination sphere, including the metal (i.e. different metals in different oxidation states) and the ligand identity (e.g. N, O or S donors; chelating ligands; etc.) [1–3]. Inspired by the active center of metalloenzymes, several research labs have developed ligand scaffolds capable of tuning the structural properties and reactivity of metal complexes by modifying their secondary coordination sphere [4–9]. One of the most common strategies is the utilization of H-bonding donors, which allows for stabilizing and characterizing metastable metal-superoxo [10], metal-hydroxperoxo [11], metal-oxo [12] and metal-hydroxo [13] species. Inspired by the seminal work of Borovik and coworkers [14,15], we have recently reported a family of metal complexes bearing bidentate ligands with tunable ureanyl H-bonding donors (Fig. 1A) [16–18]. Single crystal X-ray diffraction analysis (SC-XRD) revealed that in the solid state, these metal complexes adopt square-planar (SP), twisted pseudo-tetrahedral (TW) or tetrahedral (TD) coordination depending on the metal utilized (Co^{II}, Ni^{II}, Cu^{II}, Zn^{II}), bidentate backbone ligand (ethylenediamine vs. *o*-phenylenediamine), H-bond donor strength (ureanyl substituents), and solvent of crystallization (DMF or DMA, see Fig. 1B). We hypothesized that the changes in geometry were driven by the formation of multicenter intramolecular H-bonding interactions, which transmit modifications at the "tertiary" coordination sphere to the secondary and primary spheres (Fig. 1A). From the analysis of the structure of 22 metal complexes, we observed general trends that allow for predicting the geometry of the metal complexes. Square-planar geometries are favored with Cu^{II} and Ni^{II} as metals with *o*-phenylenediamine systems using DMF as solvent of crystallization. Twisted pseudo-tetrahedral geometry (twisted, TW) is

Abbreviations: DMF, Dimethylformamide; DMA, Dimethylacetamide; EPR, Electron paramagnetic resonance; NMR, Nuclear magnetic resonance; SC-XRD, Single-crystal X-ray diffraction; UV–vis, Ultra-violet visible; DFT, Density-functional theory; SP, Square-planar; TW, Twisted pseudo-tetrahedral; TD, Tetrahedral; α_{TW}, twist angle.

* Corresponding authors at: University of Girona, Campus Montilivi (Ciències), IQCC, Girona, Spain. ICREA, Pg. Lluís Companys 23, 08010 Barcelona, Spain.
E-mail addresses: marcel.swart@udg.edu (M. Swart), igarciab@andrew.cmu.edu (I. Garcia-Bosch).

https://doi.org/10.1016/j.ica.2023.121844
Received 13 July 2023; Received in revised form 6 November 2023; Accepted 8 November 2023
Available online 13 November 2023

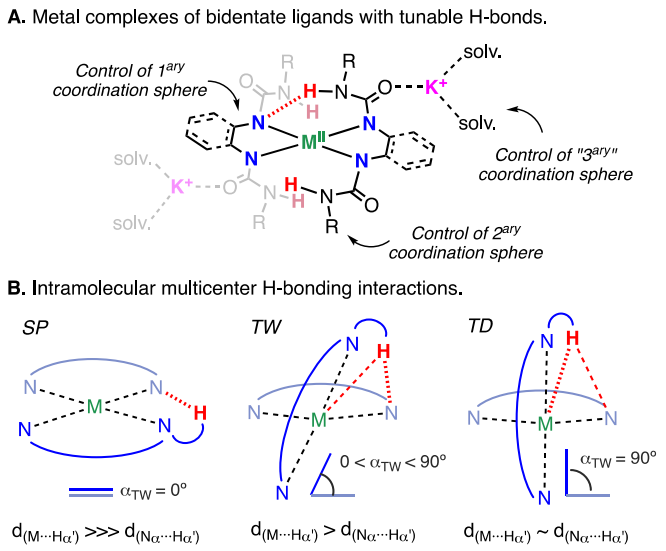

Fig. 1. (A) Primary, secondary and tertiary coordination sphere of metal complexes derived from bidentate ligands with tunable H-bond donors. (B) Intramolecular H-bonding interactions in square-planar (SP), twisted pseudo-tetrahedral (TW) and tetrahedral (TW) geometry.

observed for Cu^{II} complexes when DMA is used as solvent of crystallization and tetrahedral geometry (TD) is favored with Co^{II} and Zn^{II}.

Of course, some interesting exceptions to these general trends were also found. We were particularly puzzled with the change in geometry for the Cu^{II} complexes derived from the ligands $^{PhPh}LH_2$ and $^{2,6\text{-X2-PhPh}}LH_2$ (X: Me, Cl, F) (Fig. 2). $^{PhPh}Cu^{II}_{(K+/DMF)}$ (see Fig. 2 for naming of complexes) adopted a square-planar geometry in DMF while crystallization in DMA produced the corresponding twisted compound, $^{PhPh}Cu^{II}_{(K+/DMA)}$. Slight variations on the substituents of the ureanyl H-bond donor (2,6-substitution of the Ph group) led to SP ($^{2,6\text{-Me2-PhPh}}Cu^{II}_{(K+/DMF)}$) or TW geometries ($^{2,6\text{-F2-PhPh}}Cu^{II}_{(K+/DMF)}$ and $^{2,6\text{-Cl2-PhPh}}Cu^{II}_{(K+/DMF)}$). In this research article, we aim to determine if changes in the ureanyl group can also dictate the geometry of complexes for metal ions that are prone to favor square-planar structures such as Ni^{II} and Pd^{II} (d^8). We will also study if changes in the primary (Cu, Ni and Pd), secondary (ureanyl substituents) and tertiary coordination sphere (cation and solvent of crystallization) can also affect the geometry of these compounds in solid state.

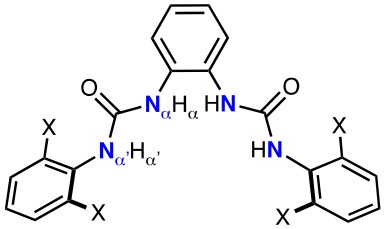

$^{PhPh}LH_2$ (X: H)
$^{2,6\text{-Me2-PhPh}}LH_2$ (X: Me)
$^{2,6\text{-F2-PhPh}}LH_2$ (X: F)
$^{2,6\text{-Cl2-PhPh}}LH_2$ (X: Cl)

	Geometry
$[Cu^{II}(^{PhPh}L^{2-})_2](K)_2(DMF)_4$ $^{PhPh}Cu^{II}_{(K+/DMF)}$	SP
$[Cu^{II}(^{PhPh}L^{2-})_2](K)_2(DMA)_6$ $^{PhPh}Cu^{II}_{(K+/DMA)}$	TW
$[Cu^{II}(^{2,6\text{-Me2-PhPh}}L^{2-})_2](K)_2(DMF)_2$ $^{2,6\text{-Me2-PhPh}}Cu^{II}_{(K+/DMF)}$	SP
$[Cu^{II}(^{2,6\text{-F2-PhPh}}L^{2-})_2](K)_2(DMF)_5$ $^{2,6\text{-F2-PhPh}}Cu^{II}_{(K+/DMF)}$	TW
$[Cu^{II}(^{2,6\text{-Cl2-PhPh}}L^{2-})_2](K)_2(DMF)_6$ $^{2,6\text{-Cl2-PhPh}}Cu^{II}_{(K+/DMF)}$	TW

Use of d^8 metals (Ni^{II}, Pd^{II}): Do they follow similar trends?
Can we control the geometry by changing the cation and/or the solvent?

Fig. 2. Ligand scaffolds and copper complexes previously reported, and summary of the studies described in this article.

2. Results and discussion

2.1. Synthesis and structural characterization of Ni and Pd complexes using K^+ as cation and DMF as solvent (ligand effect on the geometry)

Following our previous work, we prepared Ni and Pd complexes derived from $^{PhPh}LH_2$ and $^{2,6\text{-X2-PhPh}}LH_2$ in DMF (Fig. 3). These were obtained via deprotonation of the ligand scaffold with 2 equiv of KH followed by addition of 0.5 equiv of the metal(II) source (see Supporting Information, S.I., for further details on synthesis and characterization of metal complexes). The metal complexes were recrystallized using DMF/Et_2O (by layering Et_2O or vapor diffusion) and their molecular structure was determined by SC-XRD (see Fig. 4). Like in the Cu complexes, the geometry of the Ni complexes was dictated by the ligand scaffold. SP geometry was observed for $^{PhPh}Ni^{II}_{(K+/DMF)}$ and $^{2,6\text{-Me2-PhPh}}Ni^{II}_{(K+/DMF)}$ (pale yellow crystals), and TW geometry for the $^{2,6\text{-F2-PhPh}}Ni^{II}_{(K+/DMF)}$ and $^{2,6\text{-Cl2-PhPh}}Ni^{II}_{(K+/DMF)}$ systems (intense red crystals). Conversely, the geometry of the Pd^{II} complexes was exclusively determined by the metal ion, with all of the ligands producing square-planar structures (all pale yellow crystals).

SC-XRD analysis of the complexes allowed interrogating the effect of the metal ion on the intramolecular H-bonding interactions. The square-planar complex $^{PhPh}Cu^{II}_{(K+/DMF)}$ showed longer M···Nα than the Ni^{II} analogue, due to the addition of one electron in the antibonding $M-d_{x2-y2}$ molecular orbital from d^8 (Ni^{II}) to d^9 (Cu^{II}).[3] As expected, the increased atomic radius of Pd^{II} led also to longer M···Nα for $^{PhPh}Pd^{II}_{(K+/DMF)}$ when compared to $^{PhPh}Ni^{II}_{(K+/DMF)}$. The square-planar Ni complexes depicted slightly shorter intramolecular Nα···Hα' distances and

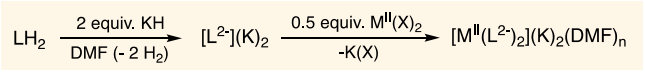

	Geometry
$[Cu^{II}(^{PhPh}L^{2-})_2](K)_2(DMF)_4$ $^{PhPh}Cu^{II}_{(K+/DMF)}$	SP
$[Cu^{II}(^{2,6\text{-Me2-PhPh}}L^{2-})_2](K)_2(DMF)_2$ $^{2,6\text{-Me2-PhPh}}Cu^{II}_{(K+/DMF)}$	SP
$[Cu^{II}(^{2,6\text{-F2-PhPh}}L^{2-})_2](K)_2(DMF)_5$ $^{2,6\text{-F2-PhPh}}Cu^{II}_{(K+/DMF)}$	TW
$[Cu^{II}(^{2,6\text{-Cl2-PhPh}}L^{2-})_2](K)_2(DMF)_6$ $^{2,6\text{-Cl2-PhPh}}Cu^{II}_{(K+/DMF)}$	TW
$[Ni^{II}(^{PhPh}L^{2-})_2](K)_2(DMF)_4$ $^{PhPh}Ni^{II}_{(K+/DMF)}$	SP
$[Ni^{II}(^{2,6\text{-Me2-PhPh}}L^{2-})_2](K)_2(DMF)_2$ $^{2,6\text{-Me2-PhPh}}Ni^{II}_{(K+/DMF)}$	SP
$[Ni^{II}(^{2,6\text{-F2-PhPh}}L^{2-})_2](K)_2(DMF)_4$ $^{2,6\text{-F2-PhPh}}Ni^{II}_{(K+/DMF)}$	TW
$[Ni^{II}(^{2,6\text{-Cl2-PhPh}}L^{2-})_2](K)_2(DMF)_6$ $^{2,6\text{-Cl2-PhPh}}Ni^{II}_{(K+/DMF)}$	TW
$[Pd^{II}(^{PhPh}L^{2-})_2](K)_2(DMF)_4$ $^{PhPh}Pd^{II}_{(K+/DMF)}$	SP
$[Pd^{II}(^{2,6\text{-Me2-PhPh}}L^{2-})_2](K)_2(DMF)_2$ $^{2,6\text{-Me2-PhPh}}Pd^{II}_{(K+/DMF)}$	SP
$[Pd^{II}(^{2,6\text{-F2-PhPh}}L^{2-})_2](K)_2(DMF)_6$ $^{2,6\text{-F2-PhPh}}Pd^{II}_{(K+/DMF)}$	SP
$[Pd^{II}(^{2,6\text{-Cl2-PhPh}}L^{2-})_2](K)_2(DMF)_3$ $^{2,6\text{-Cl2-PhPh}}Pd^{II}_{(K+/DMF)}$	SP

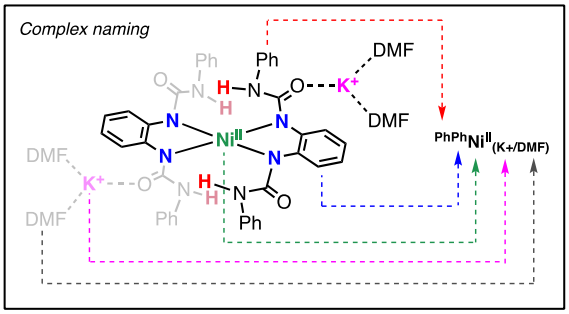

Fig. 3. Synthesis, naming and geometry of the metal complexes obtained in DMF with K^+ as countercations. See S.I. for further details.

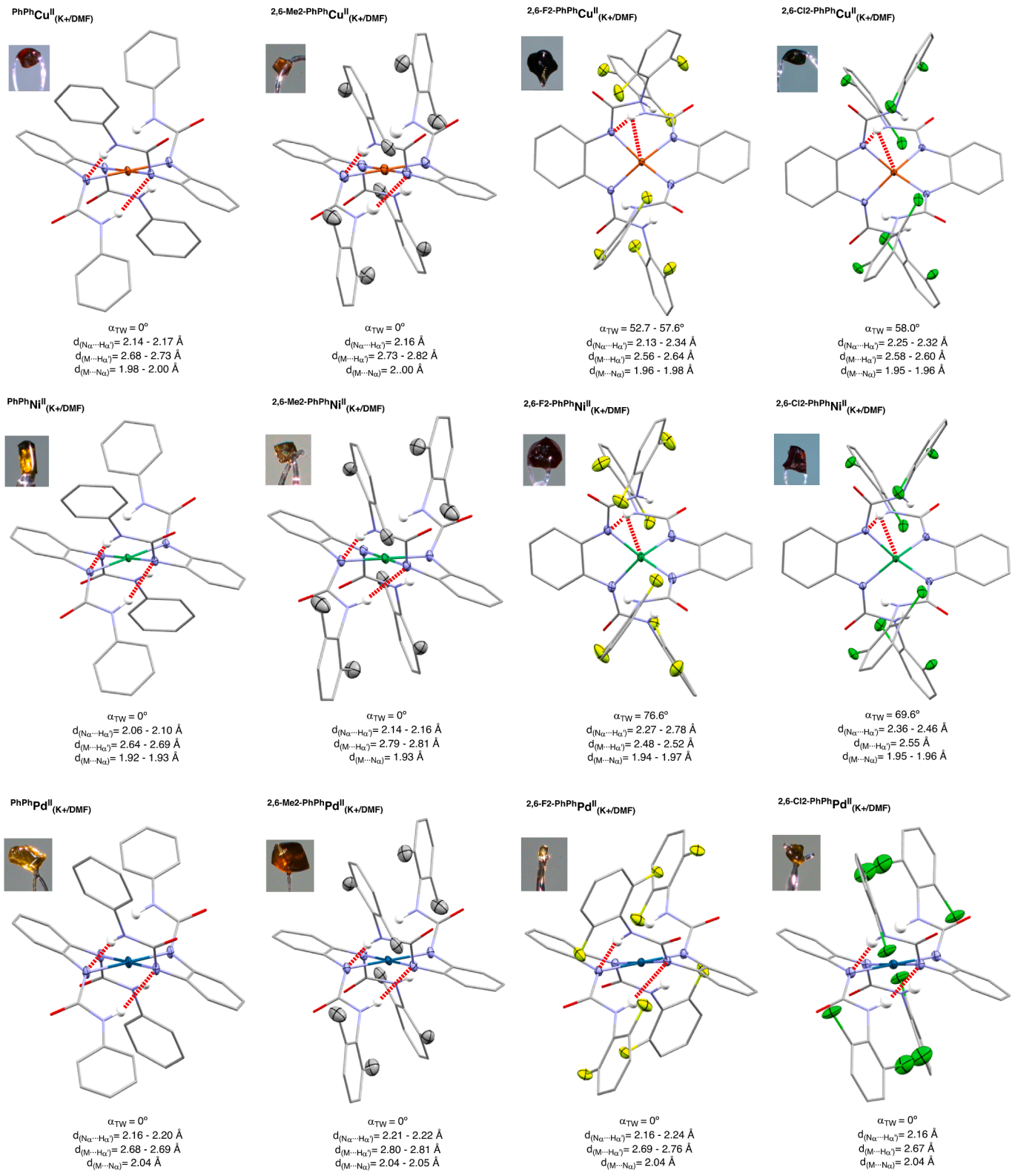

Fig. 4. SC-XRD analysis of the Cu, Ni and Pd complexes crystallized in DMF and containing K^+ as countercations. Note: the K^+ countercations, some of the H atoms and the solvent molecules were not depicted for clarity. Displacement ellipsoids are depicted at 50 % probability level for the M (M = Cu, Ni and Pd), the four coordinated N atoms and the X = Me, F, Cl. See S.I. for further details.

M···Hα' distances than the Cu and Pd analogues.

As we have previously shown, the twisted Cu and Ni complexes led to longer Nα···Hα' distances and short M···Hα' distances when compared with the square-planar analogues [17]. The twisted Ni complexes were found to adopt geometries with higher twist angles than the Cu analogues, which led to shorter M···Hα' distances and longer Nα···Hα' distances.

The fact that all of the Pd complexes adopted square-planar conformation permitted analyzing the effect of the 2,6-substitution on the geometric parameters. To our surprise, similar M···Hα' distances and Nα···Hα' distances were found for all four complexes with the only exception of $^{2,6\text{-Me2-PhPh}}\mathbf{Pd}^{II}_{(K+/DMF)}$, which depicted longer intramolecular H-bonding distances.

2.2. Synthesis and structural characterization of Cu, Ni and Pd complexes using K^+ as cation and DMA as solvent

We have previously found that the SC-XRD structure of $[Cu^{II}(^{PhPh}L^{2-})_2](K)_2$ was square-planar when crystallized in DMF ($^{PhPh}\mathbf{Cu}^{II}_{(K+/DMF)}$) and twisted pseudo-tetrahedral in DMA ($^{PhPh}\mathbf{Cu}^{II}_{(K+/DMA)}$) [16]. The color of the Cu^{II} complexes in different geometries is also revealing, being SP pale orange and TW intense purple, which allow assessing their structure with the naked eye (Fig. 4). The Ni^{II} and Pd^{II} complexes derived from $^{PhPh}LH_2$ were also synthesized using DMA, and we found that in both cases the complexes adopted SP geometries ($^{PhPh}\mathbf{Ni}^{II}_{(K+/DMA)}$ and $^{PhPh}\mathbf{Pd}^{II}_{(K+/DMA)}$). Like in the Cu complexes, the color of the Ni and Pd complexes also depends on the geometry, with the square-planar Ni^{II} and Pd^{II} systems pale yellow and the twisted Ni^{II} systems intense red (Fig. 4). The Cu complexes derived from $^{2,6\text{-Me2-PhPh}}L^{2-}$, $^{2,6\text{-F2-PhPh}}L^{2-}$ and $^{2,6\text{-Cl2-PhPh}}L^{2-}$ were also synthesized in DMA and purple complexes were obtained (see Fig. 4). This is indicative of formation of TW structures and follows the trend previously reported (i.e. SP geometries are generally stabilized with DMF, TW geometries with DMA). Not surprisingly, the synthesis of the Pd^{II} complexes in DMA did not lead to the formation of TW species due to the tendency of $4d^8$ metals to adopt SP geometries. However, changing solvent for the Ni^{II} complexes led to unexpected findings. For example, $^{2,6\text{-F2-PhPh}}\mathbf{Ni}^{II}_{(K+/DMF)}$ was crystallized as a TW complex, but $^{2,6\text{-F2-PhPh}}\mathbf{Ni}^{II}_{(K+/DMA)}$ was SP. Interestingly, $^{2,6\text{-Cl2-PhPh}}\mathbf{Ni}^{II}_{(K+/DMA)}$ produced a mixture of crystals with two different colors (pale yellow and red), corresponding to the SP and TW species.

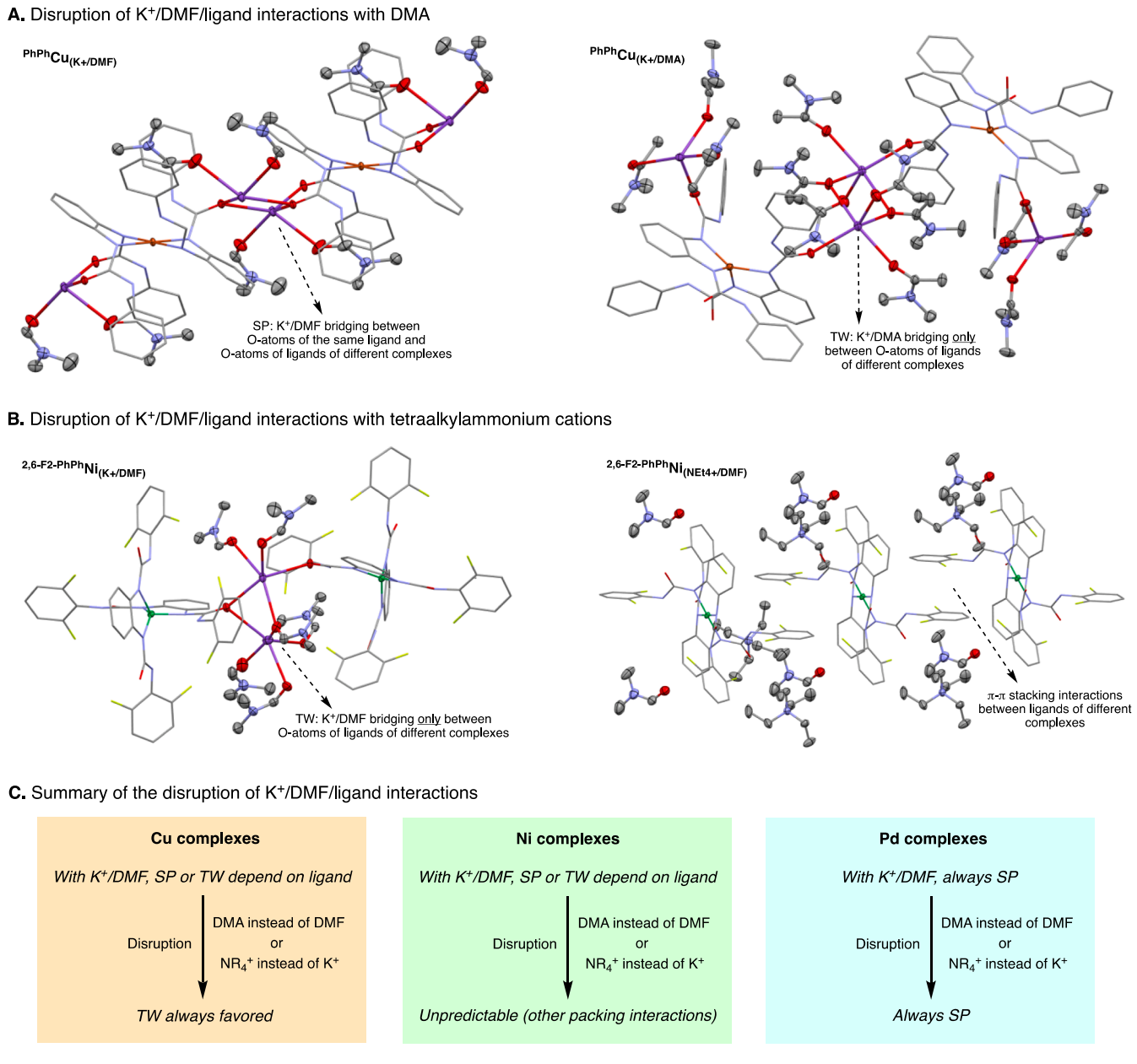

Fig. 6. SC-XRD structures depicting the disruption of the intramolecular H-bonding interactions upon changing the solvent of crystallization (A) or upon changing the counteraction of crystallization (B), and summary of the effect of disrupting intramolecular interactions for the Cu, Ni and Pd complexes. Displacement ellipsoids are drawn at the 50% probability level for atoms / moieties of interest.

We have previously analyzed the packing of the Cu complexes crystallized with K^+ as countercation and DMF or DMA as solvents. We found that in general, in the square-planar Cu complexes crystallized in DMF (e.g. $^{PhPh}Cu^{II}_{(K+/DMF)}$, $^{2,6\text{-Me2-PhPh}}Cu^{II}_{(K+/DMF)}$) the K^+ cations were bound to two O atoms of the ureanyl substituents of the same ligand and to O atoms of the ureanyl substituents of two different complexes. We also showed that in the twisted Cu structures in DMF (e.g. $^{2,6\text{-F2-PhPh}}Cu^{II}_{(K+/DMF)}$) or DMA (e.g. $^{PhPh}Cu^{II}_{(K+/DMA)}$), the K^+ cations coordinated only with one of the ureanyl substituents without acting as bridge between ligands of different complexes. We hypothesized that the disruption of the K/DMF/ureanyl interactions when DMA was used as solvent (or when varying the ureanyl substituents) led to of the crystallization of Cu complexes in TW geometry.

Herein, we found that the K^+/DMF/ureanyl interactions for the square-planar complexes $^{PhPh}Ni^{II}_{(K+/DMF)}$, $^{2,6\text{-Me2-PhPh}}Ni^{II}_{(K+/DMF)}$, $^{PhPh}Pd^{II}_{(K+/DMF)}$ and $^{2,6\text{-Me2-PhPh}}Pd^{II}_{(K+/DMF)}$ are analogous to the ones found in $^{PhPh}Cu^{II}_{(K+/DMF)}$ (see Fig. 6A). The use of DMA also disrupted the intra-ligand K^+/ureanyl bonds but only led to twisted structures for complex $^{2,6\text{-F2-PhPh}}Ni^{II}_{(K+/DMA)}$, partially for $^{2,6\text{-Cl2-PhPh}}Ni^{II}_{(K+/DMF)}$ (mixture of SP/TW) while $^{PhPh}Ni^{II}_{(K+/DMA)}$ and $^{PhPh}Pd^{II}_{(K+/DMF)}$ remained square-planar.

2.3. Synthesis and structural characterization of Cu, Ni and Pd complexes using tetraalkylammonium cations and DMF as solvent

To further disrupt the interactions between the K^+, solvent and bidentate ligands, we synthesized the metal complexes using tetralkylammonium salts as countercations (NMe_4^+ and NEt_4^+). As we hypothesized, replacing K^+ for NR_4^+ cations also led to changes in the geometry of the complexes (Fig. 5). For example, $^{PhPh}Cu^{II}_{(NEt4+,DMF)}$ was crystallized as a purple complex with TW geometry, suggesting that the presence of K^+ and DMF are critical for crystallizing $^{PhPh}Cu^{II}_{(K+,DMF)}$ in the SP

A. Synthesis of complexes in DMA with K^+ as cation.

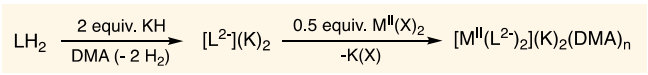

B. Synthesis of complexes in DMF and tetraalkylammonium ions as cations.

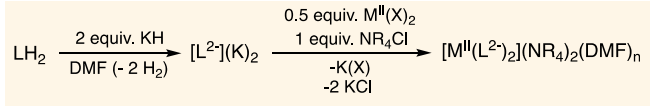

C. Geometry of the complexes upon solvent and/or cation modification

	K^+/DMF	K^+/DMA	NMe_4^+/DMF	NEt_4^+/DMF
$^{PhPh}Cu^{II}$	*SP* (X-Ray)	*TW* (X-Ray)	*TW* (X-Ray)	*TW* (X-Ray)
$^{2,6\text{-Me2-PhPh}}Cu^{II}$	*SP* (X-Ray)	*TW* (purple)	*n.d.*	*TW* (X-Ray)
$^{2,6\text{-F2-PhPh}}Cu^{II}$	*TW* (X-Ray)	*TW* (purple)	*n.d.*	*TW* (purple)
$^{2,6\text{-Cl2-PhPh}}Cu^{II}$	*TW* (X-Ray)	*TW* (X-Ray)	*n.d.*	*TW* (purple)
$^{PhPh}Ni^{II}$	*SP* (X-Ray)	*SP* (X-Ray)	*SP* (X-Ray)	*SP* (X-Ray)
$^{2,6\text{-Me2-PhPh}}Ni^{II}$	*SP* (X-Ray)	*SP* (yellow)	*n.d.*	*TW* (red)
$^{2,6\text{-F2-PhPh}}Ni^{II}$	*TW* (X-Ray)	*SP* (X-Ray)	*n.d.*	*SP* (X-Ray)
$^{2,6\text{-Cl2-PhPh}}Ni^{II}$	*TW* (X-Ray)	*SP/TW* (X-Ray)	*SP/TW* (yellow+red)	*SP/TW* (yellow+red)
$^{PhPh}Pd^{II}$	*SP* (X-Ray)	*SP* (X-Ray)	*SP* (X-Ray)	*SP* (X-Ray)
$^{2,6\text{-Me2-PhPh}}Pd^{II}$	*SP* (X-Ray)	*SP* (pale orange)	*n.d.*	*SP* (pale orange)
$^{2,6\text{-F2-PhPh}}Pd^{II}$	*D4h* (X-Ray)	*SP* (pale orange)	*n.d.*	*SP* (pale orange)
$^{2,6\text{-Cl2-PhPh}}Pd^{II}$	*D4h* (X-Ray)	*SP* (pale orange)	*n.d.*	*SP* (pale orange)

Fig. 5. Synthesis of the metal complexes obtained in DMA with K^+ as countercation (A) or in DMF with tetraakylammonium cations (B), and geometry that the complexes adopt under different crystallization conditions (C). See S.I. for further details.

geometry. Similar behavior was observed for the $^{2,6\text{-Me2-PhPh}}Cu^{II}$ complex: $^{2,6\text{-Me2-PhPh}}Cu^{II}_{(NEt4+,DMF)}$ was isolated in the TW geometry while $^{2,6\text{-Me2-PhPh}}Cu^{II}_{(K+,DMF)}$ in SP.

For $^{PhPh}Ni^{II}$, we observed that crystallization using NMe_4^+ and NEt_4^+ as cations did not lead to the formation of TW geometry ($^{PhPh}Ni^{II}_{(DMF/K+)}$, $^{PhPh}Ni^{II}_{(DMA/K+)}$, $^{PhPh}Ni^{II}_{(DMF/NMe4+)}$ and $^{PhPh}Ni^{II}_{(DMF/NEt4+)}$ are all SP). Conversely, we found that $^{2,6\text{-F2-PhPh}}Ni^{II}_{(NEt4+/DMF)}$ crystallized as SP while $^{2,6\text{-F2-PhPh}}Ni^{II}_{(K+/DMF)}$ was TW. Like in $^{2,6\text{-Cl2-PhPh}}Ni^{II}_{(K+/DMA)}$, we found that $^{2,6\text{-Cl2-PhPh}}Ni^{II}_{(NEt4+/DMF)}$ also produced a mixture of SP and TW complexes (yellow + red crystals). Closer inspection of the Ni and Pd complexes derived from $^{2,6\text{-F2-PhPh}}L^{2-}$ and $^{2,6\text{-Cl2-PhPh}}L^{2-}$ revealed π-π interactions between ureanyl substituents of two different complexes, which have not been previously observed for the Cu analogues (see Fig. 6B).

In summary, we found that disrupting the K^+/DMF/ligand interactions in the Cu systems led to selective crystallization of the complexes in TW geometry. Conversely, the Ni systems were less predictable since other packing effects (e.g. π-π stacking) emerged upon disrupting the K^+/DMF/ligand interactions. For Pd, all of the structures obtained were SP.

2.4. Intramolecular H-bonding interactions in solid state. Scattergrams

In one of our previous reports, we analyzed the intramolecular H-bonding interactions of a series of metal complexes (1 Co, 1 Ni, 20 Cu and 1 Zn complex) using the scattergram depicted in Fig. 7A.[17] We showed that the length of the intramolecular N···Hα' and M···Hα' distances depended on the geometry of the metal complexes, with the SP complexes depicting short N···Hα' and long M···Hα', and elongation of the N···Hα' and shortening of the M···Hα' distances in the TW and TD structures.

With the 22 crystal structures included in our previous publication and the 21 structures reported herein, we built updated scattergrams (see Fig. 7B-7F), which include a total of 43 complexes (see Table S43 in the S.I. to find the average values of the various parameters used to build the scattergrams). In the scattergram depicted in Fig. 7B, we observed that the square-planar Ni complexes depicted shorter N···Hα' distances than the Cu and the Pd analogues. In comparison with the twisted Cu complexes, the TW Ni complexes showed longer N···Hα' distances (similar to the pseudo-tetrahedral Zn and Co complexes).

The correlation between the intramolecular H-bonding distances and the M···Nα distances was analyzed using the scattergrams 7C and 7D. Scattergram 7C depicts the non-correlation between the M···Nα distances and the M···Hα' distances. For example, the square-planar Pd and Ni complexes showed similar M···Hα' distances while having the shortest (Ni) and the longest (Pd) M···Nα distances of the series. Similar conclusions can be drawn from scattergram 7D, in which the M···Nα distances did not correlate with the N···Hα'. An interesting aspect of scattergrams 7C and 7D is the variations of the M···Nα bonds upon modification of the metal and the geometry. For example, the square-planar Ni complexes showed shorter M···Nα distances than the twisted Ni systems, in agreement with the d^8 electrons occupying metal–ligand orbitals with bonding character for the SP and occupying metal–ligand orbitals with non-bonding character for the TW. An opposite trend was found for the Cu complexes in which shorter M···Nα are observed for the TW systems, in agreement with the occupation of metal–ligand antibonding orbitals in SP d^9 compounds.

The correlation between the intramolecular H-bonding distances and the twist angle (α_{TW}) was analyzed using the scattergrams 7E and 7F. While no correlation between the twist angle and the M···Hα' distance was found (Fig. 7F), a clear linear correlation between the twist angle and the N···Hα' distances can be drawn (Fig. 7E), with the pseudo-tetrahedral complexes having higher twist angles and longer N···Hα' distances (ca. 90°, 2.6 A) than the TW Ni (ca. 65-75°, 2.5A) and the TW Cu analogues (ca. 45-60°, 2.3 A).

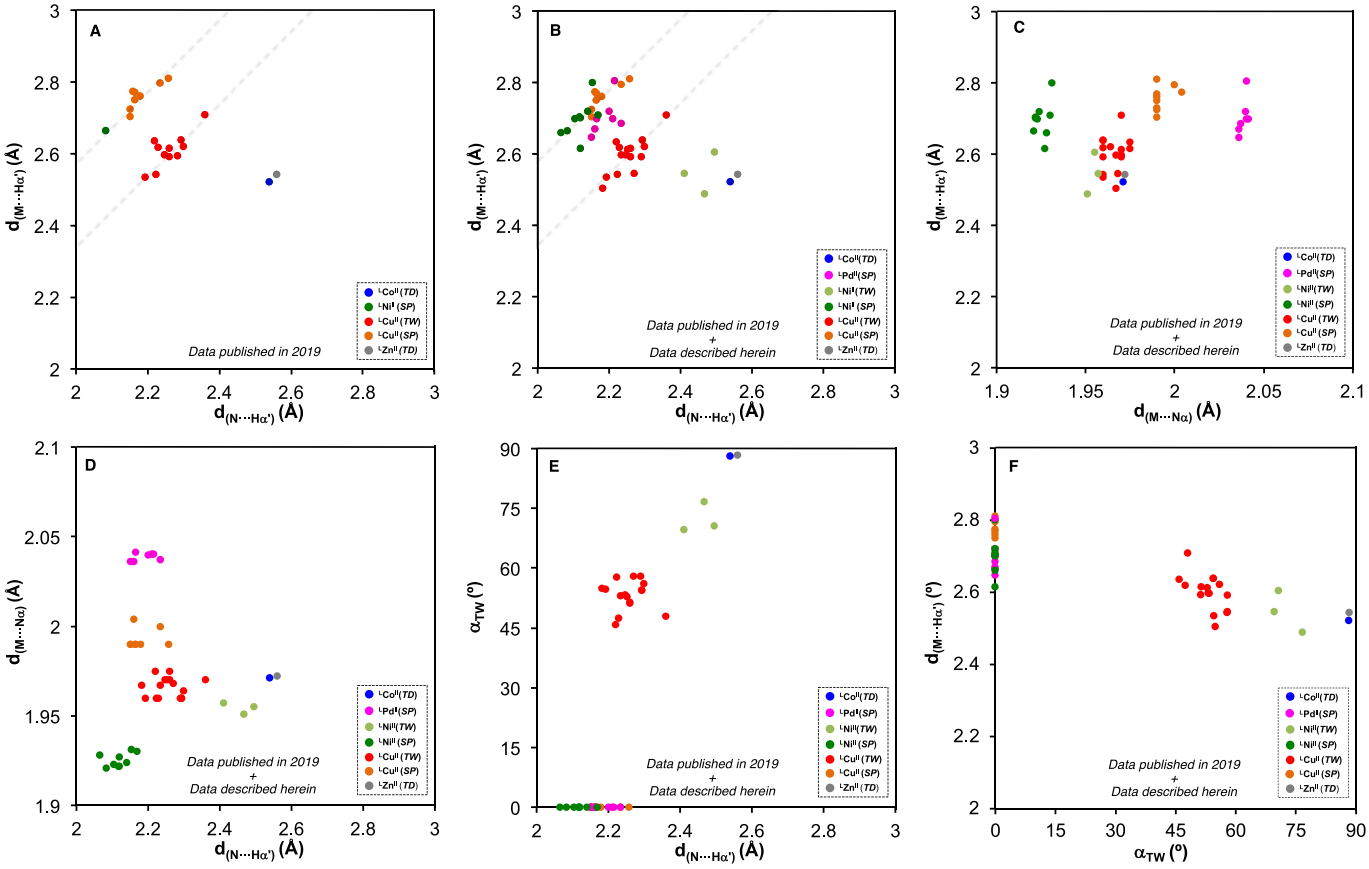

Fig. 7. Scattergram diagrams in which average M···Nα, M···Hα', M···Nα, twist angles α_{TW} are plotted against each other. Note: scattergram A was previously reported by our research group and contained crystallographic data of 22 metal complexes (1 Co, 1 Ni, 19 Cu and 1 Zn complex). Scattergrams B-F contained the crystallographic data of our previous publication (22 metal complexes) and the data included in this article (21 crystal structures).

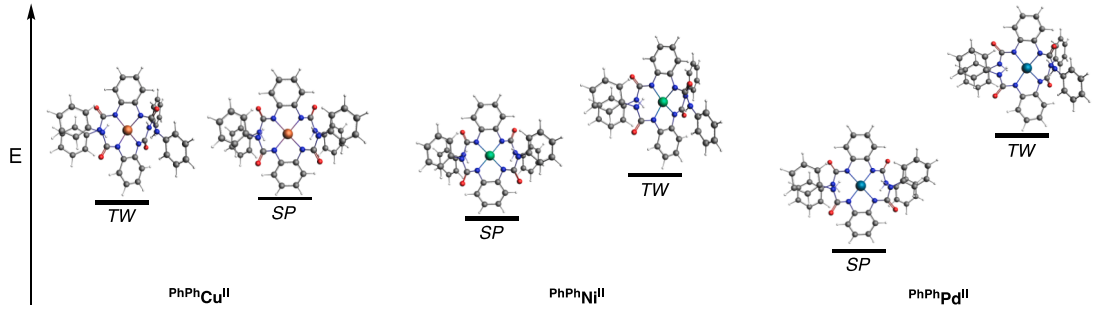

	SP $^{PhPh}Cu^{II}$ DFT (XRD)	TW $^{PhPh}Cu^{II}$ DFT (XRD)	SP $^{PhPh}Ni^{II}$ DFT (XRD)	TW $^{PhPh}Ni^{II}$ DFT (XRD)	SP $^{PhPh}Pd^{II}$ DFT (XRD)	TW $^{PhPh}Pd^{II}$ DFT (XRD)
$d(N_\alpha\cdots H_{\alpha'})$ (Å)[a]	1.98 (2.15)	2.34 (2.30)	1.97 (2.08)	2.26	2.21 (2.18)	2.20
$d(M\cdots H_{\alpha'})$ (Å)[a]	2.57 (2.70)	2.42 (2.62)	2.55 (2.66)	2.34	2.55 (2.69)	2.50
$d(M\cdots N\alpha)$ (Å)[a]	2.01 (1.99)	1.98 (1.96)	1.93 (1.92)	1.96	2.06 (2.04)	2.08
α_{TW} (°)	0 (0)	61.59 (56.03)	0 (0)	72.40	0 (0)	34.06
ΔE (TW - SP) (kcal/mol)	-	-0.64	-	6.11	-	14.22
$<S^2>$ (unpaired e^-)	0.75 (0.75)	0.75 (0.75)	0.00 (0.00)	2.00	0.00 (0.00)	0.00

Notes: [a]Average distances.

Fig. 8. DFT calculations of the square-planar and twisted isomers for $^{PhPh}Cu^{II}$, $^{PhPh}Ni^{II}$ and $^{PhPh}Pd^{II}$. Top: Enthalpic differences between the square-planar and twisted isomers (TW-SP gap). Bottom: comparison between the geometric parameters for the square-planar and twisted isomers obtained by X-ray diffraction analysis or obtained by DFT calculations. See S.I. for further details.

2.5. DFT calculations on the structure of Cu, Ni and Pd complexes in SP and TW geometry

Computations of the Cu, Ni and Pd complexes bound by $^{PhPh}L^{2-}$ and $^{2,6\text{-}X2\text{-}PhPh}L^{2-}$ in square-planar and twisted geometries were carried out (see DFT structures of $^{PhPh}Cu^{II}$, $^{PhPh}Ni^{II}$, $^{PhPh}Pd^{II}$ complexes in Fig. 8, see also S.I.). Our calculations are in close agreement with the molecular structure of the complexes obtained by XRD, depicting intramolecular H-bonding interactions (N···Hα' and M···Hα'). Like in the XRD data, the computed M···Nα distances varied depending on the metal (Cu, Ni, Pd) and geometry (SP, TW), with the SP Ni complexes depicting the shortest M···Nα distances and increasing following the series SP Ni < TW Ni < TW Cu < SP Cu < SP Pd. Our computations also predict that the intramolecular N···Hα' distances are shorter for SP complexes and that corresponding TW compounds, and that the N···Hα' distances increase with the twist angle.

In terms of energy difference between the TW and SP isomers, the Cu complexes depicted the smallest TW/SP gap, with the TW geometry slightly lower favored (Fig. 8). The energy difference between the TW and the SP isomers varied modestly within the series (between 0.6 and 1.7 kcal/mol), with $^{PhPh}Cu^{II}$ having the smallest TW-SP gap (see S.I.). Contrarywise, for the Ni complexes the SP geometry was lower in energy than the TW. The energetic gap between the SP and TW did not depend on the ligand scaffold (i.e. the $^{PhPh}Ni^{II}$ system had a similar TW-SP gap than $^{2,6\text{-}X2\text{-}PhPh}Ni^{II}$ systems, see S.I.). A similar behavior was observed for the Pd^{II} complexes, in which the SP isomers were more stable than the TW isomers but with a higher TW-SP energetic gap (~10–15 kcal/mol).

Overall, our calculations align with the experimental data obtained in the solid state (XRD). For the Cu systems, the small energy difference favoring the TW isomer agrees with the isolation of the Cu^{II} complexes in both geometries (most Cu complexes are isolated as TW). For Ni systems, the increase of the TW-SP gap favoring the SP geometry is consistent with most of the Ni complexes as SP compounds. For Pd, the big TW-SP enthalpic gap agrees with the isolation of the Pd^{II} compounds only in the SP form.

3. Conclusions

In this research article, we synthesized a series of Cu, Ni and Pd complexes bearing bidentate ligands with tunable H-bonding donors. The structures of the metal complexes in the solid state were studied by single crystal X-ray crystallography and we found that the intramolecular H-bonding interactions and the bonds between the countercation, ligand scaffold and solvent of crystallization play a critical role in favoring square-planar and/or twisted geometries. Our current research efforts are focused on studying the structure of the complexes in solution.

4. Author statement

All persons who meet authorship criteria are listed as authors, and all authors certify that they have participated sufficiently in the work to take public responsibility for the content, including participation in the concept, design, analysis, writing, or revision of the manuscript.

Declaration of Competing Interest

The authors declare the following financial interests/personal relationships which may be considered as potential competing interests: Isaac Garcia-Bosch reports financial support was provided by National Science Foundation.

Data availability

No data was used for the research described in the article.

Acknowledgments

We thank the Robert A. Welch Foundation (grant N-1900-20190330 to I.G.B.), the National Science Foundation (Grant No. [1941220] to I.G.B.), AEI/MCIU (PID2020-114548GB-I00 to M.S.) and FEDER (UNGI10-4E-801 to M.S.) for financial support. We would like to thank Prof. Michael P. Hendrich and Karl H. D. Schulz for their assistance with EPR and NMR measurements.

Appendix A. Supplementary data

Supplementary data to this article can be found online at https://doi.org/10.1016/j.ica.2023.121844.

References

[1] A.L. Balch, R.H. Holm, Complete electron-transfer series of the [M-N4] type, J. Am. Chem. Soc. 88 (22) (1966) 5201–5209.
[2] H. Basch, H.B. Gray, Molecular orbital theory for square-planar metal halide complexes, Inorg. Chem. 6 (2) (1967) 365–369.
[3] E.I. Solomon, D.E. Heppner, E.M. Johnston, J.W. Ginsbach, J. Cirera, M. Qayyum, M.T. Kieber-Emmons, C.H. Kjaergaard, R.G. Hadt, L. Tian, Copper active sites in biology, Chem. Rev. 114 (7) (2014) 3659–3853.
[4] Dahl, E. W.; Kiernicki, J. J.; Zeller, M.; Szymczak, N. K. Hydrogen Bonds Dictate O2 Capture and Release within a Zinc Tripod. *J. Am. Chem. Soc.* **2018**.
[5] S.A. Cook, A.S. Borovik, Molecular Designs for Controlling the Local Environments around Metal Ions, Acc. Chem. Res. 48 (8) (2015) 2407–2414.
[6] C.J. Chang, L.L. Chng, D.G. Nocera, Proton-Coupled O-O Activation on a Redox Platform Bearing a Hydrogen-Bonding Scaffold, J. Am. Chem. Soc. 125 (7) (2003) 1866–1876.
[7] A.J. Kendall, L.N. Zakharov, J.D. Gilbertson, Synthesis and stabilization of a monomeric iron(II) hydroxo complex via intramolecular hydrogen bonding in the secondary coordination sphere, Inorg. Chem. 49 (19) (2010) 8656–8658.
[8] Z. Thammavongsy, I.P. Mercer, J.Y. Yang, Promoting proton coupled electron transfer in redox catalysts through molecular design, Chem. Commun. 55 (70) (2019) 10342–10358.
[9] S.A. Cook, J.A. Bogart, N. Levi, A.C. Weitz, C. Moore, A.L. Rheingold, J.W. Ziller, M.P. Hendrich, A.S. Borovik, Mononuclear complexes of a tridentate redox-active ligand with sulfonamido groups: structure, properties, and reactivity, Chem. Sci. 9 (31) (2018) 6540–6547.
[10] D.E. Diaz, D.A. Quist, A.E. Herzog, A.W. Schaefer, I. Kipouros, M. Bhadra, E. I. Solomon, K.D. Karlin, Impact of intramolecular hydrogen bonding on the reactivity of cupric superoxide complexes with O−H and C−H substrates, Angew. Chem. Int. Ed. 58 (49) (2019) 17572–17576.
[11] A. Wada, M. Harata, K. Hasegawa, K. Jitsukawa, H. Masuda, M. Mukai, T. Kitagawa, H. Einaga, Structural and spectroscopic characterization of a mononuclear hydroperoxo-copper(II) complex with tripodal pyridylamine ligands, Angew. Chem. Int. Ed. 37 (1998) 798–799.
[12] C.E. Macbeth, A.P. Golombek, V.G. Young, C. Yang, K. Kuczera, M.P. Hendrich, A. S. Borovik, O-2 activation by nonheme iron complexes: A monomeric Fe(III)-oxo complex derived from O-2, Science 289 (5481) (2000) 938–941.
[13] T. Wu, S.N. MacMillan, K. Rajabimoghadam, M.A. Siegler, K.M. Lancaster, I. Garcia-Bosch, Structure, spectroscopy, and reactivity of a mononuclear copper hydroxide complex in three molecular oxidation states, J. Am. Chem. Soc. 142 (28) (2020) 12265–12276.
[14] C.E. MacBeth, P.L. Larsen, T.N. Sorrell, D. Powell, A.S. Borovik, A bidentate ligand with appended hydrogen bond donors: synthesis and structure of four-coordinate metal complexes with bis[(tert-butyl)aminocarbonyl]-1,2-diaminoethane, Inorg. Chim. Acta 341 (2002) 77–84.
[15] D. Powell-Jia, J.W. Ziller, A.G. DiPasquale, A.L. Rheingold, A.S. Borovik, A structure and reactivity analysis of monomeric Ni(II)-hydroxo complexes prepared from water, Dalton Trans. 16 (2009) 2986–2992.
[16] K. Rajabimoghadam, Y. Darwish, U. Bashir, D. Pitman, S. Eichelberger, M. A. Siegler, M. Swart, I. Garcia-Bosch, Catalytic aerobic oxidation of alcohols by copper complexes bearing redox-active ligands with tunable H-bonding groups, J. Am. Chem. Soc. 140 (48) (2018) 16625–16634.
[17] K. Rajabimoghadam, Y. Darwish, U. Bashir, D. Pitman, S. Eichelberger, M. A. Siegler, I. Garcia-Bosch, Tunable intramolecular multicenter H-bonding interactions in first-row metal complexes bearing bidentate redox-active ligands, J. Coord. Chem. 1335–1346 (2019).
[18] T. Wu, K. Rajabimoghadam, A. Puri, D.D. Hebert, Y.L. Qiu, S. Eichelberger, M. A. Siegler, M. Swart, M.P. Hendrich, I. Garcia-Bosch, A 4H+/4e– electron-coupled-proton buffer based on a mononuclear Cu complex, J. Am. Chem. Soc. 144 (37) (2022) 16905–16915.